J Am Oil Chem Soc (2008) 85:1127–1134
DOI 10.1007/s11746-008-1298-7

ORIGINAL PAPER

Fibrils of γ-Oryzanol + β-Sitosterol in Edible Oil Organogels

Arjen Bot · Ruud den Adel · Eli C. Roijers

Received: 14 August 2008 / Accepted: 17 September 2008 / Published online: 21 October 2008

Abstract Mixtures of γ-oryzanol and β-sitosterol are able to form transparent organogels in edible oils. Small-angle X-ray scattering was used to elucidate the microstructure of the building blocks of these organogels in sunflower oil. It was found that the plant sterol(ester)s form hollow tubes with a diameter of 7.2 ± 0.1 nm. Tubes prepared with γ-oryzanol-rich structurant show the least bundle aggregation, and can be supercooled during formation most easily. The tubes melt at elevated temperatures, in agreement with the loss of structuring capacity as observed in earlier experiments.

Keywords Organogel · Phytosterol · Self assembly · Fibril · X-ray diffraction (XRD) · Small-angle X-ray scattering (SAXS) · Wide-angle X-ray scattering (WAXS) · Differential scanning calorimetry (DSC)

Introduction

Low molecular weight structuring agents that can serve as an alternative to crystallising triglycerides in edible oils have raised considerable interest in recent years [1]. The requirement that potential structurants should at least hold the promise to be allowed in food applications is a severe limitation. Nevertheless, several systems have been identified, which can be grouped in two classes: single components and mixed systems.

A. Bot (✉) · R. den Adel · E. C. Roijers
Unilever Research and Development Vlaardingen,
Olivier van Noortlaan 120, 3133 AT Vlaardingen,
The Netherlands
e-mail: arjen.bot@unilever.com

Examples of single components that are capable of structuring edible oils are diglycerides, monoglycerides and fatty acids [1–7], wax esters, sorbitan monostearates, ceramides, waxes, fatty alcohols, dicarboxylic acids and derivatised fatty acids [8–16]. Examples of mixed systems are fatty acids + fatty alcohols [16–18], lecithin + sorbitan tristearate [19] and phytosterols + γ-oryzanol [20].

Despite having a similar functionality, the structuring mechanism of these systems is rather diverse. Many systems are based on the well-known crystallisation behaviour of the saturated fatty acid chains that also plays a role in regular triglyceride crystallisation [21, 22]. In some cases, this type of crystallisation leads to the formation of interesting crystal morphologies, such as fibre-like crystals [6, 7]. In the plethora of diversity, however, one system stands out as rather different: mixtures of plant sterols with γ-oryzanol [1, 20]. The systems are quite transparent up to high concentrations, and the components do not contain any of the saturated fatty acids that are responsible for crystallisation in most other systems. In fact, their chemical characteristics correspond much more with those of a number of cholesterol-derived systems investigated extensively by other groups in non-triglyceride solvents [23–27]. Those systems are known to form thin fibrils. Thin fibrils would explain the transparency of the mixed plant sterol(ester) systems.

Because direct microscopic assessment of systems in triglyceride oil was considered to be fraught with difficulties as a result of the similarity between solvent and structurant (but note recent advances by Rogers et al. [15] in this area), small-angle scattering was identified as the most straightforward technique to establish the microstructure of the building blocks in the β-sitosterol + γ-oryzanol organogels [28–31]. This paper reports on small-angle X-ray scattering (SAXS) experiments performed at the small-angle X-ray facility at the Grenoble synchrotron.

Experimental Procedures

Sample Preparation

In the present experiments γ-oryzanol ([11042-64-1], 45.9% 24-methylene cycloartenyl ferulate, 26.8% cycloartenyl ferulate, 13.1% campesteryl ferulate, 7.1% sitosteryl ferulate, 1.4% Δ^5-avenasteryl ferulate, 1.3% stigmasteryl ferulate, 1.0% campestanyl ferulate, ex Tsuno Rice Fine Chemicals Co, Wakayama, Japan) and β-sitosterol ([83-46-5], 78.5% β-sitosterol, 10.3% β-sitostanol, 8.7% campesterol, 0.9% campestanol, ex Acros) were used in combination with refined sunflower oil (6.4% C16:0, 3.4% C18:0, 20.2% C18:1cis, 67.7% C18:2cis, 0.1% C18:3cis, 0.2% C20:0, 0.6% C22:0; 0% MAG, 1.7% DAG, 98.3% TAG, ex Cargill). The chemical structures of the main components in γ-oryzanol and β-sitosterol are given in Fig. 1, and one should note that the chemical structures of the minor components in either ingredient are very similar to the main component. Earlier work confirmed that most closely related sterols show comparable gelling behaviour in edible oils [20]. Sitosterol is a minor component of many vegetable oils, including soy bean oil [32]. Oryzanol is a minor component of rice bran oil, and is an ester of ferulic acid with a range of closely related plant sterols [33].

Warm, clear stock solutions of 16% β-sitosterol and γ-oryzanol in sunflower oil were prepared, and similar 8% stock solutions were prepared by diluting part of the 16% stock solutions in an equal amount of warm sunflower oil. By mixing appropriate ratios of the stock solutions, samples were made with β-sitosterol:γ-oryzanol ratios of 100:0, 80:20, 60:40, 40:60, 20:80 and 0:100 at 8% or 16% total sterol + sterol ester concentration. The samples were cooled and stored overnight at 5 °C and stored for 1 week at 20 °C.

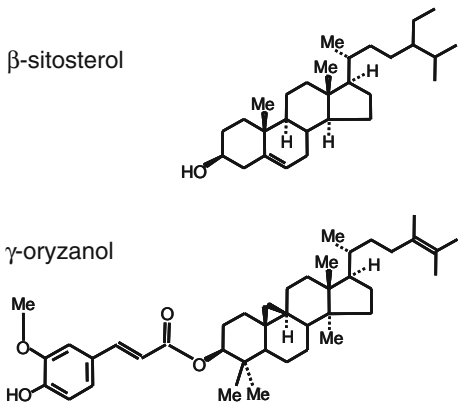

Fig. 1 Molecular structure of the main components of γ-oryzanol and β-sitosterol; the main component of γ-oryzanol is 24-methylene cycloartenyl ferulate

X-ray Scattering

Small-angle and wide-angle X-ray scattering (SAXS and WAXS, respectively) experiments were performed at the high-brilliance ID2 beamline of the European Synchrotron Radiation Facility (ESRF) in Grenoble, France [34]. The incident X-ray wavelength λ was 0.0996 nm for all experiments. The sample to detector distance was 1.50 m (SAXS) and 0.110 m (WAXS), allowing collection of SAXS data in the range $0.06 < q/\mathrm{nm}^{-1} < 4.5$ and WAXS data in the range $3.8 < q/\mathrm{nm}^{-1} < 37.8$, where $q = 4\pi\cdot\sin\theta/\lambda$ is the wave vector (and θ the scattering angle).

The samples were 2.2 mm thick, and were held in an aluminium cell with thin mica windows. Temperature (20 or 50 °C) was controlled by Peltier elements.

Data were acquired using a chip charge-coupled device camera detector. The incident and transmitted X-ray beam intensities were recorded with each SAXS pattern, and used to normalise the measured SAXS intensities. The normalized two-dimensional SAXS patterns were azimuthally averaged to obtain the scattered intensity as a function of q. The corresponding background intensity was subtracted, and the resulting corrected scattered intensity is denoted by $I(q)$.

Differential Scanning Calorimetry

Differential Scanning Calorimetric (DSC) experiments were performed using a Perkin-Elmer Pyris 1. Aluminum sample pans were filled with 15–30 mg organogel, and sealed and loaded in the DSC machine. DSC traces were obtained using a scanning rate of 10 °C/min applying a heating–cooling–heating cycle.

Results and Discussion

Diffraction Patterns of Powder and Dispersions in Oil

Figure 2 shows the diffractograms for β-sitosterol (top curve) and γ-oryzanol powder (bottom curve), featuring pronounced Bragg peaks. For β-sitosterol these can be found at $d = 2\pi/q_i = 3.76$, 3.57, 1.88, 1.78, 1.19, 0.90, 0.59, 0.52 and 0.48 nm. The slope of the scattering intensity $I(q)$ of the powders at low angles is proportional to q^{-4}.

A comparison of the powder data with results by Christiansen et al. [35] indicates that the compound is a mixture of anhydrous β-sitosterol (pronounced Bragg peaks at $d = 1.76$, 1.17, 0.88, 0.59, 0.52 nm) and β-sitosterol hemihydrate (peaks at $d = 1.88$ and 0.48 nm). The β-sitosterol hydrate would have shown an additional peak at $d = 0.50$ nm. The SAXS peaks at $d = 3.76$ and 3.57 nm

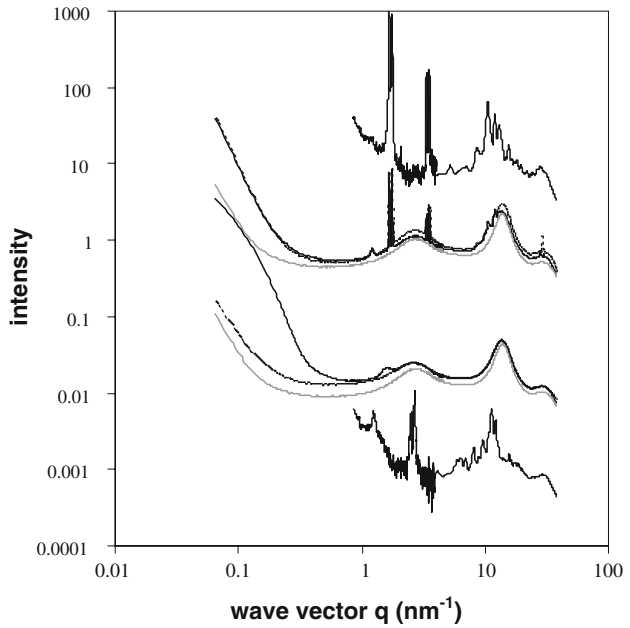

Fig. 2 Uncorrected SAXS and XRD diffractograms at 20 °C from top to bottom: β-sitosterol powder; β-sitosterol in sunflower oil (16% *solid line*, 8% *dashed line*, 0% *grey line*); γ-oryzanol in sunflower oil (16% *solid line*, 8% *dashed line*, 0% *grey line*); γ-oryzanol powder. The diffractograms are the superposition of results for a SAXS and WAXS experiment, and the data were not corrected for the presence of sunflower oil. The diffractograms were shifted vertically for clarity

in the present experiment fall outside the range that was accessible to Christiansen et al.

Bragg peaks for γ-oryzanol appear at $d = 4.95$, 2.50, 2.34, 0.99, 0.90, 0.77, 0.65, 0.58, 0.56, 0.52 and 0.40 nm. No comparable data on the diffraction patterns of γ-oryzanol was found in the literature.

Dispersion of the powder in warm oil leads upon cooling to solutions or dispersions of the plant sterol(ester). The system is liquid and does not form a gel (cf. [20]). Figure 2 also shows the diffraction patterns for β-sitosterol (top-middle set of three curves) and γ-oryzanol (bottom-middle set of three curves) in sunflower oil at three concentrations (0, 8 and 16%). Note that some sedimentation of crystals in the supersaturated solution is expected to occur during the experiment, and that the diffractograms of the solutions of the pure components should not be expected to be completely quantitative in terms of peak intensities. For the present purpose, the qualitative changes due dispersion of the plant sterol(ester)s is more important, however.

It can be seen that most of the γ-oryzanol remains dissolved in the oil at 20 °C, with only a small, relatively broad weak peak at 1.61 nm^{-1} as a new feature. This peak was not investigated further because it occurs only in the diffractograms of the (non-gelling) sterol–esters in oil and not in the gelling mixed sterol + sterol ester systems that are the centre of focus for most of the remainder of this paper. Sitosterol at high concentrations is not completely soluble in the oil at room temperature and Bragg reflections can be detected which coincide with the reflections identified in the powder spectrum, next to a weak broad feature at 1.35 nm^{-1}. This peak was not further identified for the same reasons as the weak feature in the γ-oryzanol solutions. Generally, the scattered intensity at small wave vectors increases upon addition of the plant sterol(ester)s to the oil. For the concentrated β-sitosterol dispersion, this reflects the presence of a large number of particles.

Organogel Formation

In this study, organogels were prepared at relatively high total sterol concentrations (8 and 16%) to ensure a high signal-to-noise ratio in the X-ray scattering experiment. For gel formation only, concentrations down to ~4% total sterols can be used [20].

Figure 3 captures the appearance of the mixtures of 8% γ-oryzanol + β-sitosterol in sunflower oil. The solutions/dispersions of the pure β-sitosterol or pure γ-oryzanol are liquid, the solutions of a mixture of sterol and sterol ester are gelled. Gels rich in γ-oryzanol are transparent; those rich in β-sitosterol are more turbid. Visual observation indicates that 20:80 and 80:20 β-sitosterol:γ-oryzanol samples show a few minor macroscopic inclusions, probably due to the separate crystallisation of very small amounts of the most abundant structurant in the system, but overall very little material is involved in this phenomenon. The situation for the 16% organogels is similar, albeit that the samples are more turbid overall. The higher transparency of γ-oryzanol-rich gels points towards either bigger building blocks in the more turbid gel, or towards

Fig. 3 Mixtures of 8% β-sitosterol + γ-oryzanol in sunflower oil in various sterol(ester) ratios. The β-sitosterol:γ-oryzanol ratio from left to right: 100:0; 80:20; 60:40; 40:60; 20:80; 0:100. Both single sterol(ester) systems in sunflower oil are liquid, the binary sterol(ester) systems in sunflower oil are gelled. The firm gelled samples were scooped near to the cap, leaving a distinct fracture pattern

aggregation of the building blocks (without change in the size of the building blocks themselves).

A limited number of DSC experiments were performed to demonstrate that the formation of the firm organogels does require some form of molecular ordering, since preliminary WAXS experiments on these organogels did not show any clear Bragg peaks. Confirmation of the occurrence of crystallisation constitutes complementary data only, since earlier rheological experiments did already provide indirect evidence for solidification of the structurant [20].

Figure 4 features a set of DSC curves for 16% sterol gels at diverse β-sitosterol:γ-oryzanol ratios during heating and cooling at relatively high scanning rates, indeed showing melting and crystallisation peaks. The curves show a pronounced asymmetric peak with a long tail towards lower temperatures, indicating that the dissolution process of the structurant starts at relatively low temperatures compared to the peak temperature. A small effect of phytosterol(ester) composition on melting temperature can be seen, 60:40 β-sitosterol:γ-oryzanol systems having the highest temperature for completion of melting. A much bigger difference can be seen between the heating and melting curves, in which the onset temperature for crystallisation dramatically decreases with increasing γ-oryzanol content. The effect is shown more explicitly in Fig. 5a. Note that the absolute transition temperature during cooling and heating are not expected to be exactly the same for any system at finite cooling/heating rates (temperatures obtained during heating are too high, during cooling too low). However, it is obvious that the gap between the temperature of complete melting obtained during heating and the onset temperature of crystallisation obtained during cooling increases with increasing γ-oryzanol content in the structurant mixture, which indicates that the organogels can be supercooled more easily at lower β-sitosterol:γ-oryzanol ratios. As was to be expected, it is even easier to supercool these systems at 8% structurant concentration (data not shown).

Typical melting enthalpies for systems containing 16% plant sterol(ester)s are plotted in Fig. 5b. The values range between 18 and 24 kJ/mol, with the maximum value found for 60:40 β-sitosterol:γ-oryzanol systems. The maximum value agrees well with the 26 $\pm$ 4 kJ/mol obtained by an indirect rheological method for a 50:50 β-sitosterol:γ-oryzanol organogel [20].

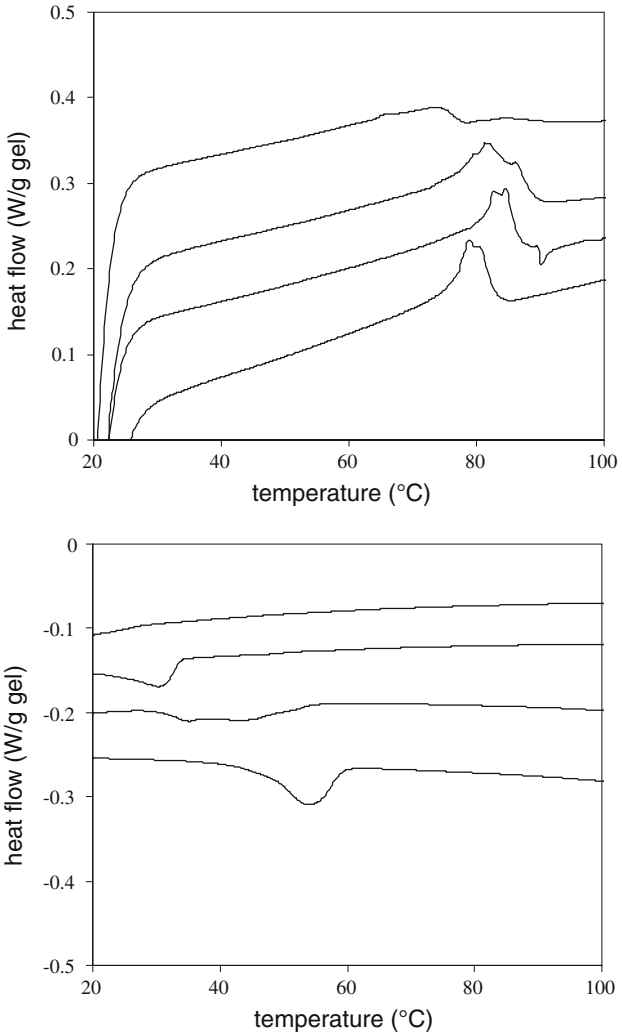

Fig. 4 Effect of β-sitosterol:γ-oryzanol ratio on the melting temperature of 16% organogels as obtained by DSC at a heating/cooling rate 10 °C/min. Curves were shifted for clarity. *Top panel* shows the heating stage, from top to bottom for 80:20, 60:40, 40:60 and 20:80 β-sitosterol:γ-oryzanol samples. *Bottom panel* shows the cooling stage with curves in inverted order (80:20 β-sitosterol:γ-oryzanol sample is the bottom curve)

Small-Angle X-ray Scattering from Organogels

Next, the organogels were subjected to an X-ray scattering experiment, resulting in overlapping SAXS and WAXS patterns. Figure 6a and b show the results after subtraction of the contribution due to the sunflower oil. The first obvious observation is the qualitative difference between the scattering patterns of the pure solutions/dispersions and the mixed systems. This correlates to the gelling behaviour of the mixtures (cf Fig. 3). The second observation is the absence of clear crystallographic order in the mixed systems (especially in the WAXS section of the diffraction pattern), except from some relatively weak peaks which should be associated with the small inclusions in the gel. On the other hand, a very pronounced interference pattern can be observed, with broad maxima at 0.99, 1.96 and 2.75 nm^{-1}. The intensity of the pattern is the highest for the 40:60 β-sitosterol:γ-oryzanol sample in the 8% total sterol sample, and for 40:60 and 60:40 in the 16% total sterol sample. The position of the maxima is not affected

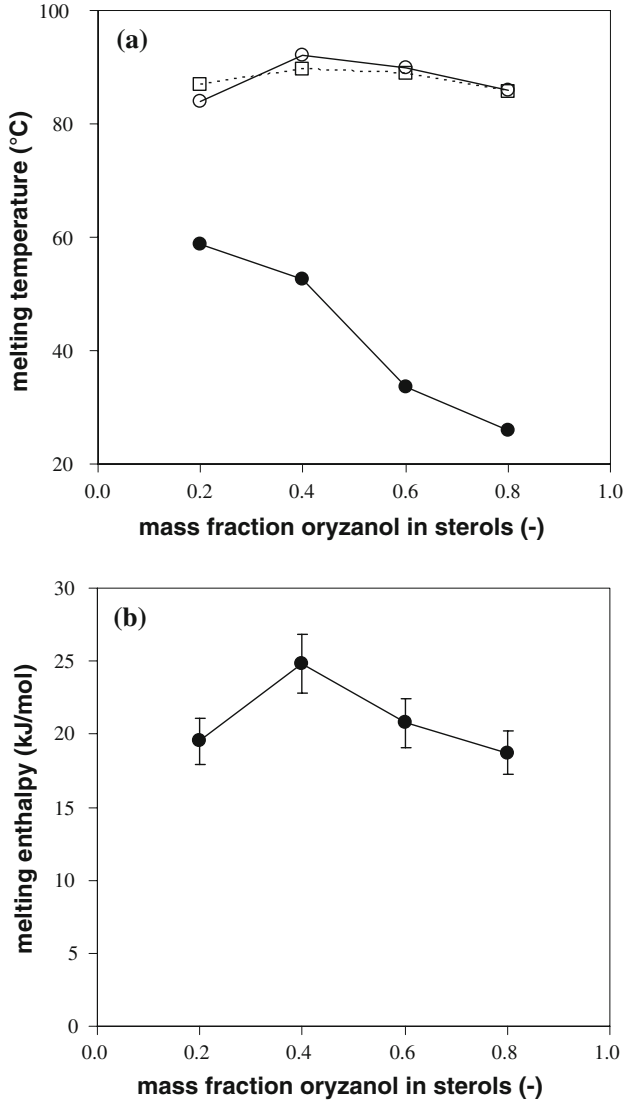

Fig. 5 Effect of β-sitosterol:γ-oryzanol ratio on the melting temperature and melting enthalpy of 16% organogels: **a** melting temperature (completion of melting during heating, onset of crystallisation during cooling; heating/cooling rate 10 °C/min), indicating an enhanced tendency to supercooling at high γ-oryzanol content, (*open circles*) first heating, (*filled circles*) first cooling, (*open squares*) second heating. *Error bars* are the same size as the *symbols*; **b** melting enthalpy as determined during the first heating curve

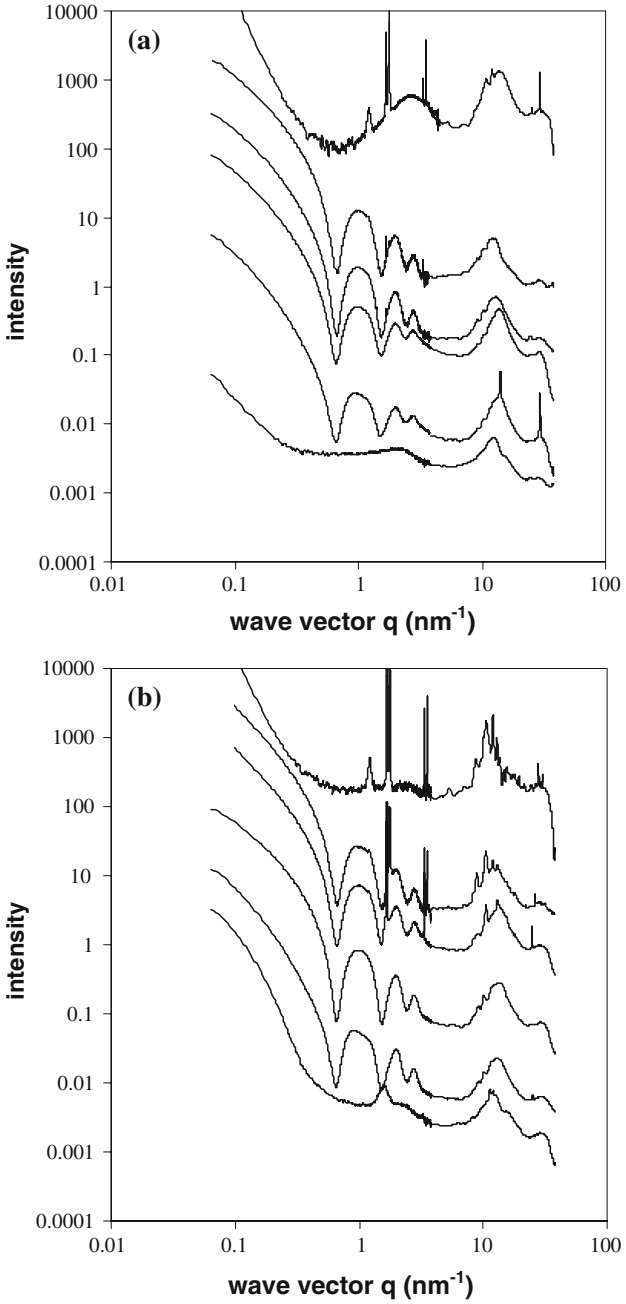

Fig. 6 SAXS and WAXS diffractograms for β-sitosterol + γ-oryzanol in sunflower oil at 20 °C in various sterol(ester) ratios: **a** 8% total sterol(ester)s; **b** 16% total sterol(ester)s. The β-sitosterol:γ-oryzanol ratio from top to bottom: 100:0; 80:20; 60:40; 40:60; 20:80; 0:100. The curves were shifted for clarity: each curve in the series 60:40, 40:60 and 20:80 was shifted by an additional factor of 10 relative to the 80:20 curve; the 100:0 curve is shifted by a factor 100,000 relative to 0:100

by total sterol(ester) concentration or the β-sitosterol:γ-oryzanol ratio. The depth of the interference minima suggest that the responsible structure is rather monodisperse (finite instrumental resolution being another factor capable of blurring sharp features). In the 8% samples the depth of the interference minima is most pronounced in the β-sitosterol-rich sample, in the 16% sample this effect is not present.

The obvious interpretation of the scattering data based on earlier rheological studies [20] would be in terms of solid cylinders, with $I(q) \sim J_1{}^2(qr_c)/q^3$ (with J_1 the first-order Bessel function, q the wave vector and r_c the radius of the cylinder) [36]. However, the data suggest that the maxima of the interference peaks decrease proportional to q^{-2}, whereas the model for solid cylinders would require a decrease proportional to q^{-4}. Confronted with a similar

situation for organogels based on cholesterol-derivatives, Sakurai et al. [23] proposed the use of the hollow cylinder model.

$$I(q) \sim J_0^2(qr_c)/q \quad (1)$$

with J_0 the zeroth-order Bessel function [36], which does indeed show the required q-dependence and fits the data very well (see Fig. 7 for a fit to the data for the 60:40 β-sitosterol:γ-oryzanol gel with 8% total sterol(ester)s). The model implies that the plant sterol(ester)s form a thin cylindrical shell with vegetable oil on the inside and outside of the shell. The diameter of the cylinder $2r_c$ is 7.2 ± 0.1 nm.

In principle, the model can be improved upon by introducing a finite wall thickness (i.e. a nanotube), $I(q) \sim (r_{out} \cdot J_1(qr_{out}) - r_{in} \cdot J_1(qr_{in}))^2/(q^3 \cdot (r_{out}{}^2 - r_{in}^2)^2)$ with r_{out} and r_{in} the outer and inner wall radius [37, 38]. The first maximum in the interference pattern remains at the same position compared to Eq. (1) provided that one chooses r_{in} and r_{out} (with $r_{in} < r_c < r_{out}$) such that the same amount of nanotube wall material can be found in a cylinder with inner and outer wall at r_{in} and r_c as in a cylinder with walls at r_c and r_{out}. It is found that peak intensities do not change much for the first three interference peaks as long as the wall thickness remains below $\sim$1.0 nm. The peak positions starts to change qualitatively beyond a wall thickness of 2 nm. An analysis of the experimental ratio of the interference peak intensities even suggests a thickness smaller than 0.6 nm, but this number is unfortunately relatively sensitive to small errors in background corrections. Therefore, it was concluded that the use of the more advanced model does not bring bigger benefits than a confirmation that the hollow cylinder model captures the essential elements of the structure, and that wall thickness seems small compared to the cylinder diameter.

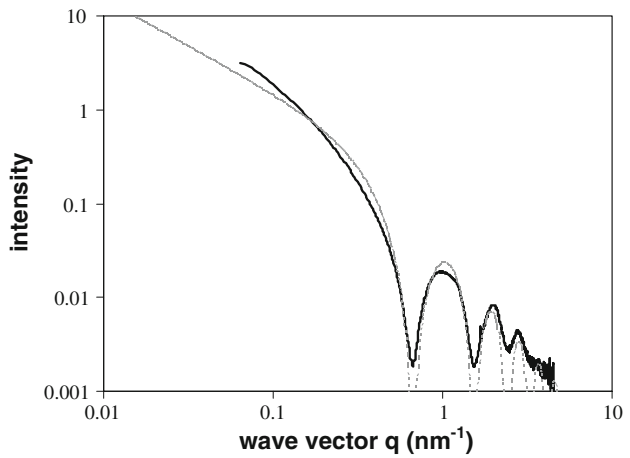

Fig. 7 SAXS pattern for β-sitosterol + γ-oryzanol in sunflower oil for a 8% total sterol(ester)s organogel with a β-sitosterol:γ-oryzanol ratio of 60:40 at 20 °C. The *dashed curve* is a fit according to the hollow cylinder model with a radius of 7.2 nm

The WAXS section of the diffractograms does not show pronounced sharp peaks, as mentioned above. However, it does show a broad peak at a similar position as for the sunflower oil peak, but apparently slightly shifted towards smaller q ($\sim$13–14 nm^{-1}). The shape of the peak is sometimes slightly distorted by apparently small errors in the background correction (due to the liquid oil peak). The data hint at a weak second broad feature at lower q ($\sim$2–3 nm^{-1}), in line with the minor features for the single component solutions in Fig. 2. This peak could possibly be partly responsible for the smaller apparent depth of the interference minima for some of the curves, especially those for samples rich in γ-oryzanol.

The interpretation of this WAXS part of the diffraction pattern is more complicated. The breadth of the features would favour an interpretation as a liquid-like ordering of the plant sterol(ester)s in the hollow cylinder. Such a random conformation would be difficult to reconcile with the rather monodisperse nature of the nanotubes as inferred from the depth of the interference minima. Therefore, the width of the peaks is interpreted here as being due to wedged stacking of the molecules, leading to a curvature in the molecular assembly. Such wedged stacking was proposed before for this system, based on crude molecular modelling [1]. The curvature prevents the system having the type of long-range translational order required for sharp reflections. This interpretation suggests that the main distance between molecules in the nanotube wall is $\sim$0.45 nm, similar to typical distances between TAG molecules in liquid oil [39].

The changes in scattering pattern with temperature are shown in Fig. 8 (after correction for the contribution of sunflower oil). It shows four pairs of diffractograms of curves obtained at 20 and 50 °C. The data shows that the effect of temperature is minor for the structure of the 16% total sterol organogels, whereas a clear loss of structure is observed for the 8% organogels. The loss in structure is bigger for the 8% 20:80 sitosterol:oryzanol mixture than for the 40:60 mixture.

Interestingly, the 8% organogels have been observed to lose their structuring potential at around 50 °C (see Fig. 9 in Ref. [20]). The results indicate that the nanotube does not persist above the melting temperature, suggesting that structuring is not caused by a mesophase (e.g. a tubular micelle) crystallising below a critical temperature, as was proposed as a possibility earlier [1]. The data support direct formation of the nanotube.

The small-angle X-ray scattering data on β-sitosterol + γ-oryzanol in sunflower oil can be interpreted in terms of the formation of nanotubes, 7.2 nm in diameter and with a wall thickness of less than 1.0 nm. The most

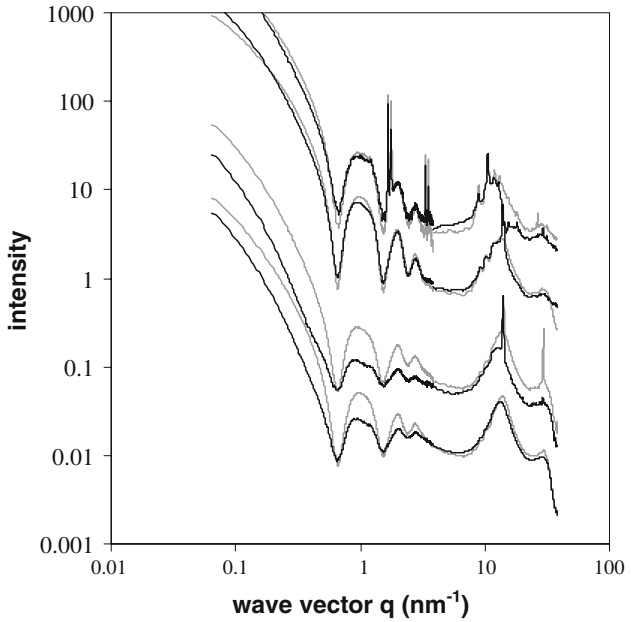

Fig. 8 Pairs of SAXS and WAXS diffractograms for β-sitosterol + γ-oryzanol in sunflower oil at 20 °C (*grey line*) and 50 °C (*black line*) at various sterol(ester) ratios. From top to bottom: 16% total sterol(ester)s, β-sitosterol:γ-oryzanol ratio 20:80; 16%, ratio 40:60; 8%, ratio 80:20; 8%, ratio 40:60. Each pair of curves was shifted by a factor 10 for clarity

likely growth mechanism for this nanotube would be via a helical ribbon, in which the wall spirals along the central axis [40], but experimental data to support this hypothesis directly is lacking as for now. Details concerning the molecular orientation of the sterol(ester)s in the wall of the nanotube are lacking too. Molecular modelling studies would be useful to develop further understanding here. Furthermore, an independent microscopic conformation of the microstructure of these fibres would be desirable.

The increase in turbidity of the plant sterol gels for mixtures rich in β-sitosterol (see Fig. 3) may indicate that interfibre aggregation is more likely to occur, whereas systems rich in γ-oryzanol suffer less from bundle formation. This would support an earlier hypothesis [1] that the ferulic acid moieties in γ-oryzanol help to keep the nanotubes apart and work as a spacer. Nanotubes prepared with γ-oryzanol-rich structurant are also found to be supercooled more easily during formation.

The properties of the β-sitosterol + γ-oryzanol organogels in edible oils place the systems clearly into the much wider category of organogels in other solvents (e.g. [28–31, 41–44]). As such, the present results may provide additional help in the identification of the critical requirements to achieve gel formation in non-aqueous liquids.

Acknowledgments The authors would like to thank T. Narayanan (ESRF) for support during experiments on the ID2 beam line in Grenoble, R. Baris (Unilever R&D) for analytical support, and W.G. Bouwman (TU Delft) for helpful discussions.

References

1. Pernetti M, van Malssen KF, Flöter E, Bot A (2007) Structuring of edible oils by alternatives to crystalline fat. Curr Opin Colloid Interface Sci 12:221–231
2. Realdon N, Ragazzi E, Ragazzi E (2001) Effect of gelling conditions and mechanical treatment on drug availability from a lipogel. Drug Develop Indust Pharm 27:165–170
3. Ojijo NKO, Neeman I, Eger S, Shimoni E (2004) Effects of monoglyceride content, cooling rate and shear on the rheological properties of olive oil/monoglyceride gel networks. J Sci Food Agric 84:1585–1593
4. Ojijo NKO, Kesselman E, Shuster V, Eichler S, Eger S, Neeman I, Shimoni E (2004) Changes in the microstructural, thermal, and rheological properties of olive oil/monoglyceride gel networks during storage. Food Res Int 37:385–393
5. Kesselman E, Shimoni E (2007) Imaging of oil/monoglyceride networks by polarizing near-field scanning optical microscopy. Food Biophys 2:117–123
6. Wright AJ, Marangoni AG (2006) Formation, structure, and rheological properties of ricinelaidic acid–vegetable oil organogels. J Am Oil Chem Soc 83:497–503
7. Wright AJ, Marangoni AG (2007) Time, temperature, and concentration dependence of ricinelaidic acid–canola oil organogelation. J Am Oil Chem Soc 84:3–9
8. Murdan S, Gregoriadis G, Florence AT (1999) Novel sorbitan monostearate organogels. J Pharm Sci 88:608–614
9. Rogers MA (2008) Nanostructuring fiber morphology in 12-HSA organogels and the development of a food grade organogelator. Thesis, University of Guelph, Canada
10. Daniel J, Rajasekharan R (2003) Organogelation of plant oils and hydrocarbons by long-chain saturated FA, fatty alcohols, wax esters, and dicarboxylic acids. J Am Oil Chem Soc 80:417–421
11. Tamura T, Suetake T, Ohkubo T, Ohbu K (1994) Effect of alkali-metal ions on gel formation in the 12-hydroxystearic acid soybean oil system. J Am Oil Chem Soc 71:857–861
12. Toro-Vazquez JF, Morales-Rueda JA, Dibildox-Alvarado E, Charo-Alonso M, González-Chávez M, Alonzo-Macias MM (2007) Thermal and textural properties of organogels developed by candelilla wax in safflower oil. J Am Oil Chem Soc 84:989–1000
13. Rogers MA, Wright AJ, Marangoni AG (2008) Post-crystallization increases in the mechanical strength of self-assembled fibrillar networks is due to an increase in network supramolecular ordering. J Phys D 41:215501
14. Rogers MA, Wright AJ, Marangoni AG (2008) Engineering the oil binding capacity and crystallinity of self-assembled fibrillar networks of 12-hydroxystearic acid in edible oils. Soft Matter 4:1483–1490
15. Rogers MA, Smith AK, Wright AJ, Marangoni AG (2007) A novel cryo-SEM technique for imaging vegetable oil based organogels. J Am Oil Chem Soc 84:899–906
16. Gandolfo FG, Bot A, Flöter E (2004) Structuring of edible oils by long-chain FA, fatty alcohols, and their mixtures. J Am Oil Chem Soc 81:1–6
17. Schaink HM, van Malssen KF, Morgado Alves S, Kalnin D, van der Linden E (2007) Crystal network for edible oil organogels: possibilities and limitations of the fatty acid & fatty alcohol systems. Food Res Int 40:1185–1193

18. Schaink HM, van Malssen KF (2007) Shear modulus of sintered 'House of Cards'-like assemblies of crystals. Langmuir 23:12682–12686
19. Pernetti M, van Malssen K, Kalnin D, Flöter E (2007) Structuring edible oil with lecithin and sorbitan tri-stearate. Food Hydrocoll 21:855–861
20. Bot A, Agterof WGM (2006) Structuring of edible oils by mixtures of γ-oryzanol with β-sitosterol or related phytosterols. J Am Oil Chem Soc 83:513–521
21. de Bruijne DW, Bot A (1999) Fabricated fat-based foods. In: Rosenthal AJ, (ed) Food texture: measurement and perception, Chap 7. Aspen, Gaithersburg, pp 185–227
22. Bot A, Flöter E, Lammers JG, Pelan EG (2007) The texture of and microstructure of spreads. In: McClements DJ (ed) Understanding and controlling the microstructure of complex foods. Woodhead Publishing, Cambridge, pp 575–599
23. Sakurai K, Ono Y, Jung HJ, Okamoto S, Sakurai S, Shinkai S (2001) Synchrotron small angle X-ray scattering from organogels Part 1 Changes in molecular assemblies of cholesterol gelators during gel-sol transition. J Chem Soc Perkin Trans II 2001:108–112
24. Wade RH, Terech P, Hewat EA, Ramasseul R, Volino F (1986) The network structure of a steroid/cyclohexane physical gel. J Colloid Interface Sci 114:442–451
25. Terech P, Furman I, Weiss RG, Bous-Laurent H, Desvergne JP, Ramasseul R (1995) Gels from small molecules in organic solvents: structural features of a family of steroid and anthryl-based organogelators. Faraday Disc 101:345–358
26. Terech P, Ostuni E, Weiss RG (1996) Structural study of cholesteryl anthraquinone-2-carboxylate (CAQ) physical organogels by neutron and X-ray small angle scattering. J Phys Chem 100:3759–3766
27. George M, Weiss RG (2006) Molecular Organogels. Soft matter comprised of low-molecular-mass organic gelators and organic liquids. Acc Chem Res 39:489–497
28. Imae T, Funayama K, Krafft MP, Giulieri F, Tada T, Matsumoto T (1999) Small-angle scattering and electron microscopy investigation of nanotubules made from a perfluoroalkylated glucophospholipid. J Colloid Interface Sci 212:330–337
29. Sakurai K, Jeong Y, Koumoto K, Friggeri A, Gronwald O, Sakurai S, Okamoto S, Inuoe K, Shinkai S (2003) Supramolecular structure of sugar-appended organogelator explored with synchrotron X-ray small-angle scattering. Langmuir 19:8211–8217
30. Krysmann MJ, Castelletto V, McKendrick JE, Clifton LA, Hamley IW, Harris PJF, King SM (2008) Self-assembly of peptide nanotubes in an organic solvent. Langmuir 24:8158–8162
31. Willemen HM, Marcelis ATM, Sudhölter EJR, Bouwman WG, Demé B, Terech P (2004) A small-angle neutron scattering study of cholic acid-based organogel systems. Langmuir 20:2075–2080
32. von Bonsdorff-Nikander A, Karjalainen M, Rantanen J, Christiansen L, Yliruusi J (2003) Physical stability of a microcrystalline β-sitosterol suspension in oil. Eur J Pharm Sci 19:173–179
33. Xu Z, Godber JS (1999) Purification and identification of components of oryzanol in rice bran oil. J Agric Food Chem 47:2724–2728
34. Narayanan T, Diat O, Bösecke P (2001) SAXS and USAXS on the high brilliance beamline at the ESRF. Nucl Instrum Meth Phys Res A 467:1005–1009
35. Christiansen LI, Rantanen JT, von Bonsdorff AK, Karjalainen MA, Yliruusi JK (2002) A novel method of producing a microcrystalline β-sitosterol suspension in oil. Eur J Pharm Sci 15:261–269
36. Fedorova IS, Schmidt PW (1978) A general analytical method for calculating particle-dimension distributions from scattering data. J Appl Crystall 11:405–411
37. Deutch JM (1981) Light-scattering from hollow finite cylinders. Macromolecules 14:1826–1827
38. Díaz N, Simon FX, Schmutz M, Rawiso M, Decher G, Jestin J, Mésini PJ (2005) Self-assembled diamide nanotubes in organic solvents. Angewandte Chem Int Edition 44:3260–3264
39. Garti N, Sato K (1988) Crystallization and polymorphism of fats and fatty acids. Marcel Dekker, New York
40. Brizard A, Oda R, Huc I (2005) Chirality effects in self-assembled fibrillar networks. In: Fages F (ed) Low molecular mass gelators, topics in current chemistry, vol 256. Springer, Berlin, pp 167–218
41. Abdallah AJ, Weiss RG (2000) Organogels and low molecular mass organic gelators. Adv Mater 12:1237–1247
42. Weiss RG, Terech P (eds) (2006) Molecular gels: materials with self-assembled fibrillar networks. Springer, Dordrecht
43. Escuder B, Miravet JF (2006) Silk-inspired low-molecular weight organogelator. Langmuir 22:7793–7797
44. Peng J, Lin K, Liu J, Zhang Q, Feng X, Fang Y (2008) New dicholesteryl-based gelators: chirality and spacer length effect. Langmuir 24:2992–3000